Acoustic emission induced by sand liquefaction during vibration loading

Vladimir Frid (vladimirf@ac.sce.ac.il)
Sami Shamoon College of Engineering
Semen Shulov
Sami Shamoon College of Engineering

Article

Keywords:

Posted Date: April 5th, 2022

DOI: https://doi.org/10.21203/rs.3.rs-1508652/v1

Abstract

The article deals with the study of poorly graded sand samples of different grain content subjected to liquefaction. Eleven parameters of acoustic emission (AE) were studied during the process of sand liquefaction. The research results show the V-shaped behavior of the AE parameters that correspond to the three-stage sand behavior associated with the changes in its stress state as follows: the behavior of AE in phase A is due to microfractures/displacements between sand grains caused by an increase in pore pressure before the liquefaction point. Phase B (the stage of AE silence just before the liquefaction point) reflects the equality between pore pressure and cell pressure. Phase C (the stage of increase in AE parameters' values) is explained by intense friction between sand grains during their movement caused by liquefaction.

Despite the obvious signs of the V-shaped behavior of the AE excitation relative to the liquefaction point, changes in the AE parameters depend on the composition of the sand. The results show that the change in the sand composition from the poorly graded dune sand to "extremely poorly graded sand" significantly increases the time for the creation of the liquefaction state while the larger the grain size, the longer the time needed to reach the liquefaction state. The last finding is explained by the increase in soil hydraulic conductivity, which complicates the conditions for the increase in pore pressure and hence makes longer the time till the liquefaction state is reached.

Introduction

The dynamic behavior of soils associated with liquefaction is an important phenomenon in the earthquake (EQ) engineering[1–3]. The rate and magnitude of pore pressure generation during EQs have an essential outcome on the soil stability, even if it does not liquefy[4]. The dynamic behavior of soils is affected by their type, the intensity of applied load, and the degree of saturation[5]. The transformation of the stress-strain to the liquefaction state follows with the intensive reduction in the initial dynamic characteristics of sands[6] while most soil deformations occur after the start of liquefaction[7]. Soil failure caused by liquefaction often takes time to develop and may occur after the earthquake has ceased[8]. Three-dimensional cyclic tests have been widely used to study the dynamic behavior of soils[9]. It was revealed that the liquefaction state occurs ~9 seconds after the initiation of the main shaking. The issue of the time of liquefaction triggering[7] was studied in the frequency domain. It was shown that the frequency content changes significantly with time during soil oscillation namely the high-frequency content appears before triggering of liquefaction and it transforms to a low-frequency oscillation after the liquefaction state was reached. The relationship between the liquefaction safety factor and the value of the maximum shear effort applied was established[10]. It was noted that this relationship is affected by the soil density and grain size distribution. The effect of relative density, the intensity of horizontal stress, and the intensity of applied oscillations were studied[11,12]. It was shown that the soil resistance to liquefaction significantly depends on a previous seismic activity[13].

Acoustic emission (AE) is a phenomenon recognized related to frictions between sand grains[14–16] that is widely applied to study the failure features of various materials including soils [e.g.,17,18]. The AE signals were registered during compaction of coarse-grained sand[19] and water penetration into sand samples[20]. The AE phenomenon induced by soil failure has been studied concerning the stability of slopes [e.g., 21–24]. The concise review of AE caused by failure of soil samples was presented in[25,26] where the phenomenon was investigated being induced by the compression of three types of soil samples (on distinct types of compression instruments) using dry and wet sands of different grain content. The state of art analysis portrays that most of the AE studies during soil compression were performed in conditions of static or quasi-static loading.

This paper presents novel results of the AE study during sand liquefaction induced by dynamic/ vibration loading. Four types of poorly graded sand are used. Our results demonstrate that grain content affects not only the likelihood of sand liquefaction but the time to reach the liquefaction state as well.

Materials And Methods

The materials and methods used in the study are described in detail in our previous articles[25,26], below we will only briefly consider these issues. The dune sand material for the study was collected in the coastal area of Ashdod (about 30 km south of Tel Aviv city, Israel). According to the Uniform Soil Classification System (USCS), the sand has an index of SP (poor grade sand). All research experiments were conducted with four types of samples: the dune sand and its three fractions, sifted as follows: 2.36–0.6, 0.6 – 0.3, 0.3–0.075 mm. The percentage of these three fractions in the content of dune sand is as follows: 50%, 45%, 3.5%, respectively. The dynamic loading system (Controls SpA., Italy) combined with the AE registration instruments were employed for the experiments (Fig. 1a). The parameters of the dynamic loading are as follows: a. The diameter and length of the sand samples are 70 and about 120 mm, respectively (Fig. 1b), b. The frequency of sinusoidal vibration – 1 Hz, c. The amplitude of vertical vibrations ± 350N (± 90 kPa), d. The initial effective pressure in the load cell – 150 kPa, e. The duration of vibrations – 100 sec.

To characterize the moment of liquefaction state, the following three parameters were studied: a. The "B" factor is the ratio of change in pore pressure (relative to the initial pore pressure) "ΔP" to the initial value of effective water pressure in the load cell - σ ', b. The value of effective horizontal stress, σ', c. The value of shear stress, $\tau = \frac{\sigma_1 - \sigma_3}{2}$, where σ_1 and σ_3 are vertical and horizontal stress values in the pressure chamber.

The procedure of sample preparation for the experiments consisted of six main stages as follows: a. The raw sand material was dried for a day in an oven at a temperature of 105°C[27], b. The sand was rolled out in a thin layer, moistened to 5% of the water content, and then heated up to 60°C for several hours. The value of 5% of the water content is the experimentally found largest amount of water that can be absorbed by a sand sample without squeezing out the water during sample compaction[25], c. Each

cylindrical sand sample was prepared in an elastic jacket (Fig. 1b). The initial value of density of wet sand samples prepared for each experiment was 1.79 ± 0.03 g/cm^3. d. The sample end cup was connected to a vacuum pump to achieve a vacuum of 100 kPa in the sample pore space, e. The initial value of water pressure in the load cell was 50 kPa, f. The sample saturation procedure was performed in the following sequential steps: f1. The Back Pressure (BP) was increased by 70 kPa, f2. The Cell Pressure (CP) was increased by 70 kPa, f3. The check of the increase in the ratio of Pore Pressure ΔPP to increase in Cell Pressure ΔCP (ΔPP/ΔCP) was performed, f4. The procedure was repeated to increase the ratio ΔPP/ΔCP to ∼0.8 meaning the sample was saturated to about 80% implying the sample is ready for the liquefaction test. The AE sensor (Fig. 1c) was connected to the “micro SHM monitoring system” (Mistras/Physical Acoustic Inc.) (Fig. 1d). The “AE win for Micro SHM” software was used for data continuous acquisition during the entire vibration loading.

Eleven parameters of AE hits were investigated as follows: a. the number of AE hits, b. the Rate of the number of AE signals - the Time between AE events per Hit Number), c. the time between the AE signals, d. the RISE-TIME - The time from the first threshold to the peak of the highest waveform (μs), e. the COUNTS - The number of times the letter AE crosses the identification threshold from the beginning of the letter to the end, f. the DURATION – The Duration of the AE pulse (μs), g. the ENERGY - The time integral of the signal voltage, h. the AMPLITUDE - The maximum value of voltage in the form of a wave AE (AE_{db}), i. the AVERAGE FREQUENCY - The value of counts divided by the length of time (parts 1000 - in units of kHz), j. the PEAK NUMBER (PCNTS) - The number of cycles that exceed the measurement threshold at the time of the rise of AE signal, k. the ABSOLUTE ENERGY - The time integral of the signal voltage at the sensor before any amplification divided by a 10kΩ impedance and expressed in aJ (attoJoules – 10^{-18} Joules)

Results

The results of geomechanical studies

Figures 2**(a-c)** show the values of factor “B”, effective stress, and shear stress, respectively, to the point in time when the liquefaction state is created.

Analysis of Fig. 2 shows that:

a. The time required for the transition of sand to a liquefied state depends on its composition. The shortest time (the highest rate) is set for dunes sand which is a mixture of three other fractions (Sect. Methods and Materials), The larger the grain size content of sand, the longer it takes to reach the liquefaction state,
b. Once the liquefaction mode is created the value of the "B" factor for all samples is similar. The maximum value of the rate of change of the "B" factor is for the sample of dune sand (Fig. 2a – blue line).

c. Approximately 10 seconds after the creation of liquefaction state, the value of the rate of change "B" factor is similar for all studied sand samples

d. The time required to reduce the horizontal effective stress values to zero depends on the composition of the sand (Fig. 2b). The shortest time was found for the dune sand samples. The larger the grain diameter of the sand samples, the longer the duration of the decrease in the values of the horizontal effective stress to zero. It should be noted that the maximum rate of the process is also determined for the dune sand. Once the liquefaction state is achieved the value of effective horizontal stress for all samples is similar.

e. The time required to decrease shear stress values depends on the composition of the sand sample as well (Fig. 2c). The shortest time is typical for the dune sand samples, which are a mixture of three fractions. Note that the maximum rate of the process is also set for sand dunes.

Results of AE studies

Figure 3 shows the values of AE Hit Number in the range of ± 30 seconds around the liquefaction point (X-axis: the number of oscillations is equal to 0). It can be seen (Fig. 3) that: a. The number of AE signals decreases before a liquefaction state is created, b. There is a certain time range of AE silence, c. The number of AE signals at the liquefaction point increases but it depends on the composition of the sand samples, d. The response of dune sand to changes in the liquefaction state is extremely intense relative to three other fractions studied.

Figures 4a-j show the changes of ten parameters of AE as follows: Fig. 4a the Rate of the number of AE signals (i.e. the Time between AE events per Hit Number), Fig. 4b - the time between the AE signals, Fig. 4c - the changes in Rise-Time of AE signals, Fig. 4d - the changes in Counts, Fig. 4e - the changes in energy, Fig. 4f - the changes in signals' duration, Fig. 4g - the changes in signals' amplitude, Fig. 4h - the changes in signals' frequency, Fig. 4i - the changes in the number of peaks in AE signals, Fig. 4j – the changes in the value of absolute energy of AE signals. From the analysis of the AE findings, the anomaly of AE occurs, usually, a few seconds before the time point of liquefaction is achieved.

A certain time before the liquefaction state has been created the value of time between AE hits decreases (Fig. 4b), sometime before the liquefaction state the AE hits disappeared, so-called silence” time, while immediately before the liquefaction point the time between successive AE hits increases again for all sand fractions. The above phenomenon indicates the formation of an equilibrium state between pore pressure and the pressure in the load cell (arrow in Fig. 4b). Analysis of Figs. 4c-j portrays that the appearance of all other AE parameters resembles that noted above, namely, their values decrease before the liquefaction point and increase again immediately when the liquefaction state is created. The example of the zone of change in Rise-time behavior is highlighted in the black ellipse in Fig. 4c. Similar behavior can be found for other parameters (e.g., Figs. 4e, h, i).

In summary, the studied AE parameters manifested themselves in three phases, resembling the letter “V” as follows: Phase A is the phase of increase in AE parameters intensity, Phase B - is the phase of AE silence before the liquefaction state is created, Phase C is the phase immediately before the creation of

the liquefaction state when the values of the parameters AE begin to increase. It can be noted that despite the similarity in the behavior of AE excitation relatively to the liquefaction point for all studied soil compositions its specific properties do depend on the sand composition.

Discussion And Conclusion

The features of the V-shaped behavior of the AE parameters can be understood by considering an example of three vibration diagrams (Fig. 5a-c) that show the changes of vibration parameters during dynamic loading of dune sand sample (Fig. 5a shows the displacement chart while Figs. 5b and 5c show the charts of vibration velocity and acceleration, respectively). The liquefaction state is created 10 seconds after the start of oscillations (”0” on the X-axis – like in Figs. 3,4). The displacement diagram can be characterized by three key features as follows: a. The amplitude of the displacement increases until a liquefaction condition is created while the slope of the graph remains unchanged, b. The slope of the displacement curve changes when the liquefaction conditions are created, c. The displacement amplitude remains quite unchangeable until the end of the test. As for the velocity and acceleration charts, their amplitude reaches its maximum value when the liquefaction state is created and does not change significantly after the liquefaction point, as does the displacement behavior. Note the similarity between the presented above parameters and the values of PGD, PGV, and PGA ($3.7*10^{-4}$-$1.0*10^{-7}$, $1.6*10^{-3}$-$8.3*10^{-7}$, $4.4*10^{-2}$-$1.2*10^{-5}$, respectively) presented in the Earthquake Catalog[28].

A comparison of three stages of displacement, velocity, and acceleration charts (Fig. 5a, b, c, respectively) with the three-phase behavior of AE parameters (Figs. 3,4) portrays that the first stage in Fig. 5 (the stage of amplitude increase in displacement, velocity, and acceleration corresponds to phase A - the phase of increase in AE parameters value - Figs. 3,4). The zone before the breaking point in graphs of displacement, velocity, and acceleration (Fig. 5) nearly corresponds to Phase B where the AE is not caused (so-called the zone of silence, Fig. 4b). Stage 3 in Fig. 5 (the stage of the unchangeable amplitude of displacement, velocity, and acceleration as well as the stage characterized by the slope change in displacement curve that is much bigger than in Stage 1 and the slope of velocity and acceleration curves quite close to 0) corresponds to Phase C where when the magnitude of AE parameters increases again.

It can be assumed that such behavior of AE in phase A is due to microfractures/displacements between sand grains caused by an increase in pore pressure. Phase B reflects the equality between pore pressure and cell pressure. The behavior of AE in phase C can be explained by intense friction between sand grains during their movement caused by liquefaction. Note that, despite the obvious signs of the V-shaped behavior of the AE excitation relative to the liquefaction point, changes in the AE parameters depend on the composition of the sand. This feature can be explained by the difference in friction between sand grains of varied sizes, which is manifested in the unequal behavior of three geo-mechanical parameters. As can be seen (Fig. 2), the behavior of the B factor, as well as the values of the effective stress and shear, are qualitatively similar. The values of the B factor increase to a value of 1, while the values of the effective stress and shear stress decrease significantly when the state of liquefaction is reached. The value of the rate of three parameters increases with approaching the liquefaction state and decreases

after the liquefaction point. However, the rate of change of these three parameters is different for each type of sand and is determined by its granular composition.

The absolute value of the rate increases with decreasing grain size, while their highest value is noted for dune sands, which are a mixture of the three studied fractions.

The noted above similarity in behavior of AE parameters (asymmetrical "V" type) implies that the change in the behavior of AE can indeed be an indicator of the approach to the liquefaction state.

Our previous studies[24,25] showed that most AE parameters are interdependent apart from the lack of the inter-correlation between two parameters: the number of AE hits and the values of absolute energy of AE hits. Such a similar character of the behavior of the studied AE parameters during liquefaction is not unexpected, but, on the contrary, indicates the consistency of the present study with the previous ones[24,25] conducted during the static loading.

The results of our vibration experiments with four different sand types show that if the pore pressure exceeds 80% of the value of effective stress, a liquefaction state will inevitably be reached, and the number of vibrations required to reach this state (or in other words, the time required to reach the liquefaction state) is highly dependent on the granular composition of the sand. For example, the time necessary to create a liquefaction state in the dune sand is only 10 seconds. This finding means that a magnitude 6–7 earthquake will cause liquefaction of dune sand. The above results are consistent with the previous ones[1]. The changes in the sand composition from the poorly graded dune sand to "extremely poorly graded sand" (consisting of a very thin range of grain sizes e.g., 2.36–0.6 mm, 0.6 – 0.3 mm, and 0.3-0.075 mm) significantly increases the time for the creation of liquefaction state. Moreover, the larger the grain size, the longer the time needed to reach the liquefaction state. Since the pore diameter is often estimated to be 20% of the D10 size (the grain size corresponding to 10% sieve passing) and since the soil hydraulic conductivity is frequently considered to be related to the value of D10, the increase in D10 value means the increase in soil hydraulic conductivity and hence the longer time required to reach significant pore pressure in the coarser-grained sand. Since the time to reach the liquefaction state is related to the duration of the vibrations caused by the earthquake and the composition of the soil at the base of the structure, the above conclusion has the potential to increase the warning time by increasing the time to create the liquefaction state and therefore creating safer conditions for structures built in the marine environment. Changes in the AE parameters observed during the study indicate the possibility of developing an early warning system for the creation of liquefaction conditions at the base of structures in the marine environment, as well as applying the above parameters to assess the integrity of offshore structures due to soil liquefaction.

The circumstances of the influence of the composition of the sand on the symmetry/asymmetry of the letter "V", as well as its amplitude and aperture, are currently not clear and will be studied in further studies.

Declarations

Acknowledgments: Authors would like to thank the Ministry of Construction and Housing of Israel for the financial support of the research (Grant 3/2019, 4501851885).

Authors' contribution: Authors declare equal contribution to all aspects of the research conducting and the article preparation.

Data Availability Statement: All data generated and analyzed during this study are included in the article.

Conflicts of Interest: The authors declare no conflict of interest.

References

1. Huang, Y. & Yu M. Review of soil liquefaction characteristics during major earthquakes of the twenty-first century. *Nat Hazards* **65**, 2375–2384 (2013).
2. Chakrabortty, P., Popescu, R. & Phillips, R. Liquefaction Study of Heterogeneous Sand: Centrifuge. *Geotechnical Testing Journal* **33(3),** 227-237 (2019).
3. Wang, C.-Y. & Manga, M. *Earthquakes and Water*. (Springer-Verlag Berlin Heidelberg, 2010).
4. Sitharam, T. G. & Govindaraju, L. Pore pressure generation in silty sands during cyclic loading. *Geomechanics and Geoengineering. An International Journal* **2(4)**, 295-306 (2007).
5. Finn, W.D.L. State of the art for the evaluation of seismic liquefaction potential. *Computers and Geotechnics* **29,** 329–341 (2002).
6. Talaganov K.V. Stress-strain transformations and liquefaction of sands. *Soil Dynamics and Earthquake Engineering* 15, 411-418 (1996).
7. Ozener P.T., Greenfield, M.W., Sideras, S.S. & Kramer, S.L. Identification of time of liquefaction triggering. *Soil Dynamics and Earthquake Engineering* **128,** 105895 (2020).
8. Jones A.L., Steven L. Kramer, S.L., Arduino, P. & Eberhard M. Uncertainty Analysis for a Seismic Warning System. *Transportation Research Record* 1808 Paper No. 02- 3774 112-121
9. Ishihara, K. & Yasuda, S. Soil liquefaction due to irregular excitation. *Soils and Foundations* **12(4)**, 65–77 (1972).
10. Tsukamoto Y., Ishihara K. & Sawada S. Settlement of silty sand deposits the following liquefaction during earthquakes. *Soils and Foundations.* **44(5),** 135–148 (2004).
11. Kumar S.S., Dey, A. & Krishna, A.M. Response of saturated cohesionless soil subjected to irregular seismic excitations. *Nat Hazards.* **93**, 509–529 (2018).
12. Kumar S.S., Krishna A.M. & Dey A. Evaluation of dynamic properties of sandy soil at high cyclic strains. *Soil Dyn. Earthq. Eng.* **99**, 157–167 (2017).
13. Abdoun, T., El-Sekelly, W. & Dobry R. Investigation of Vs – based liquefaction charts using a heavily preshaken silty sand centrifuge deposit. *Soil Dynamics and Earthquake Engineering*. **122** 39–52

(2019).

14. Andreotti, B. Sonic sands. **Rep. Prog. Phys. 75,** 026602 1-24 (2012).
15. Dutta, K. Singing Sand Dunes. *Resonance.* April, 339-351 (2016).
16. Michlmayr, G., Cohen, D. & Or, D. Sources and characteristics of acoustic emissions from mechanically stressed. *Earth-Sci. Rev.* **112**, 97–114 (2012).
17. Lin, W., Liu, A., Mao, W. & Koseki, J. Acoustic emission characteristics of a dry sandy soil subjected to drained triaxial compression. *Acta Geotech*. 2020, doi:10.1007/s11440-020-00932-w.
18. Naderi-Boldaji, M., Bahrami, M., Keller, T. & Or, D. Characteristics of acoustic emissions from soil subjected to confined uniaxial compression. *Vadose Zone J.,* **16,** 2017, doi:10.2136/vzj2017.02.0049.
19. Fernandes, F., Syahrial, A. I. & Valdes J. R. Monitoring the Oedometric Compression of Sands with Acoustic Emissions. *Geotechnical Testing Journal*. **33(5),** 410-415 (2019).
20. Hung, M.-H., Lauchle, G.C. & Wang, M. Seepage-Induced Acoustic Emission in Granular Soils. *Journal of geotechnical and geoenvironmental engineering*. **135**, 566-572 (2009).
21. Smith, A., Dixon, N. & Fowmes, G.J. Early detection of first-time slope failures using acoustic emission measurements: Large-scale physical modeling. *Géotechnique* 67, 138–152 (2017), doi:10.1680/jgeot.15. P.200.
22. Smith, A., Dixon, N., Meldrum, P., Haslam, E. & Chambers, J. Acoustic emission monitoring of a soil slope: Comparisons with continuous deformation measurements. *Geotechnique Lett.* **4**, 255–261 (2014).
23. Deng, L., Yuan, H., Chen, J., Sun, Z., Fu, M., Zhou, Y., Yan, S., Zhang, Z., Chen, T. Experimental investigation on progressive deformation of soil slope using acoustic emission monitoring. *Eng. Geol.* 261, 105295 (2019).
24. Hu, W., Scaringi, G., Xu, Q. & Huang, R. Acoustic emissions and microseismicity in granular slopes before failure and flow-like motion: The potential for early warning. *Geophys. Res. Lett.* **45**, 10,406–10,415 (2018).
25. Frid V., Potirakis S.M. & Shulov S. Study of Static and Dynamic Properties of Sand under Low Stress Compression. *Applied Sciences. MDPI*, **11**, 3311 (2021) doi.org/10.3390/app11083311.
26. Frid V., Potirakis S.M. & Shulov S. Effect of Soil Loading and Unloading on its Acoustic Behavior. *Proceedings* **67**, 20 (2020) doi:10.3390/ASEC2020-07516.
27. ASTM D4959 – 00. Standard Test Method for Determination of Water (Moisture) Content of Soil by Direct Heating; ASTM International: West Conshohocken, PA, USA, 2016.
28. Yagoda-Biran, G., Maiti, S., Wetzler, K., Nof, R. N., Pashcur, Y. & Kamai, R. A Ground-Motion Database for Israel with Its Corresponding Point-Source Parameters, for Engineering Seismology Applications, *Seismol. Res. Lett.* **92**, 2679–2690 (2021).
29. Rosas, J., Lopez, O., Missimer, T. M., Coulibaly, K.M., Dehwah, A.H.A., Sesler, K., Lujan, L.R. & Mantilla, D. Determination of Hydraulic Conductivity from Grain-Size Distribution for Different Depositional

Environments. *Groundwater* **52(3)**, 399–413 (2014).

Figures

Figure 1

The research instruments: a. The dynamic loading system (Controls SpA., Italy), b. The sand sample: diameter and length are 70 and about 120 mm, respectively, c. The AE sensor d. The “micro SHM monitoring system” (Mistras/Physical Acoustic Inc.)

Figure 2

Three geomechanical parameters which characterize the liquefication state are as follows: a. the values of the “B” factor, b. the value of effective stress, c. the value of shear stress, the X-values is the number of vibration cycles while 0 when the B factor value is reached to 1 (the negative values mean the state before the liquefaction point while the positive values after the liquefaction point), the Y-axis is the value of the corresponding measured parameter. The blue, green, black, and red lines are for dune sand, fractions 2.36-0.6, 0.6-0.3, 0.3-0.075 mm, respectively

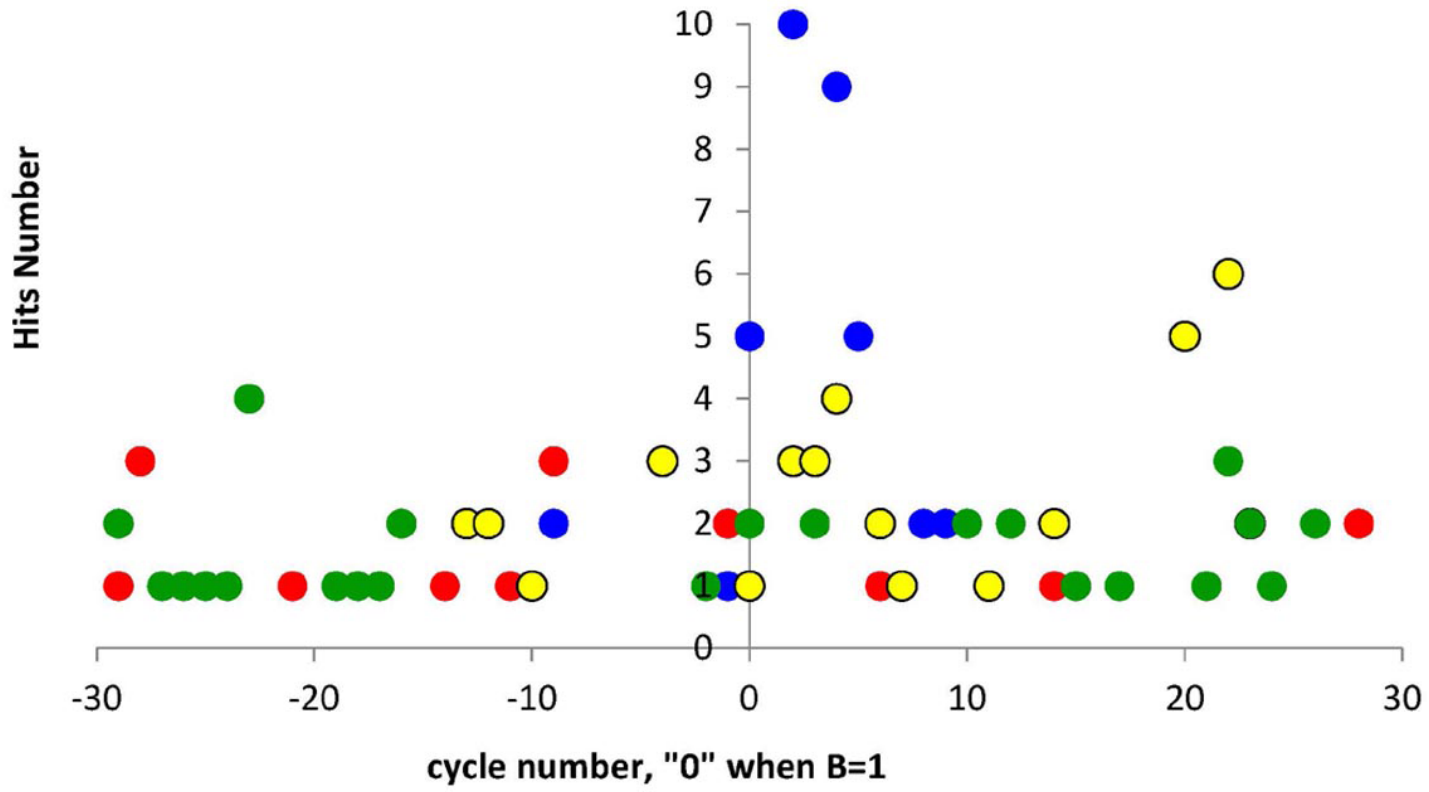

Figure 3

The changes in AE hit number before and after the liquefaction state is created, the X-values is the number of vibration cycles while 0 when the B factor value is reached to 1, the Y-axis is the value of AE hit number. The blue, green, yellow-black, and red circles are for dune sand, fractions 2.36-0.6, 0.6-0.3, 0.3-0.075 mm, respectively

Figure 4

Ten AE parameters are as follows: a. The rate of the number of AE signals (i.e., The Time between AE events per the Hit Number), b. the time between the AE signals, c. The change in the Rise-Time of AE signals, d. The change in Counts, e. The change in energy value, f. The change in signals' duration, g. The change in signals' amplitude, h. The change in signals' frequency, i. The change in the number of peaks in AE signals, j. The change in the value of absolute energy of AE signals, the X-values is the number of vibration cycles while 0 when the B factor value approaches the value equal to 1, the Y-axis is the value of corresponding AE number, the blue, green, yellow-black, and red circles are for dune sand, fractions 2.36-0.6, 0.6-0.3, 0.3-0.075 mm, respectively

Figure 5

Legend not included with this version